

Article

# Oxidation of Sulfamethoxazole by Rice Husk Biochar-Activated Persulfate

Efstathios Avramiotis <sup>1</sup>, Zacharias Frontistis <sup>2</sup>, Ioannis D. Manariotis <sup>3</sup>, John Vakros <sup>1,\*</sup> and Dionissios Mantzavinos <sup>1</sup>

<sup>1</sup> Department of Chemical Engineering, University of Patras, Caratheodory 1, GR-26504 Patras, Greece; e.avramiotis@upatras.gr (E.A.); mantzavinos@chemeng.upatras.gr (D.M.)

<sup>2</sup> Department of Chemical Engineering, University of Western Macedonia, GR-50100 Kozani, Greece; zaxoys@gmail.com

<sup>3</sup> Environmental Engineering Laboratory, Department of Civil Engineering, University of Patras, GR-26504 Patras, Greece; idman@upatras.gr

\* Correspondence: vakros@chemistry.upatras.gr

**Abstract:** In the present study, biochars from rice husk were synthesized via pyrolysis at 400, 550, 700 and 850 °C for 1 h under a limited O<sub>2</sub> atmosphere, characterized with a various techniques of and used as catalysts to activate persulfate and to degrade sulfamethoxazole (SMX). After physicochemical characterization of biochars. SMX degradation tests were performed using different water matrices, persulfate biochar and SMX concentrations and different initial pH solutions. Also, spiked solutions with bicarbonate, chloride, calcium nitrate, humic acid or alcohols were tested. It was found that catalytic reactivity rises with the pyrolysis temperature. Biochar is crucial for the oxidation of SMX and it can be described with a pseudo first-order kinetic model. Real matrices hinder the oxidation process, in waste water the SMX removal is 41% in 90 min, comparable with the inhibition obtained with spiked with bicarbonates solution (52% removal within 90 min) while complete removal can be achieved in ultrapure water matrices. The presence of alcohol slightly inhibits degradation contrary to the addition of sodium azide which causes significant inhibition, this is an evidence that degradation either under electron transfer/singlet oxygen control or dominated by surface-bound radicals.

**Keywords:** biochar; rice husk; sodium persulfate; advanced oxidation processes; wastewater; sulfamethoxazole



**Citation:** Avramiotis, E.; Frontistis, Z.; Manariotis, I.D.; Vakros, J.; Mantzavinos, D. Oxidation of Sulfamethoxazole by Rice Husk Biochar-Activated Persulfate. *Catalysts* **2021**, *11*, 850. <https://doi.org/10.3390/catal11070850>

Academic Editor: Marta Pazos Currás

Received: 30 June 2021

Accepted: 14 July 2021

Published: 15 July 2021

**Publisher's Note:** MDPI stays neutral with regard to jurisdictional claims in published maps and institutional affiliations.



**Copyright:** © 2021 by the authors. Licensee MDPI, Basel, Switzerland. This article is an open access article distributed under the terms and conditions of the Creative Commons Attribution (CC BY) license (<https://creativecommons.org/licenses/by/4.0/>).

## 1. Introduction

In the last few decades, biomass valorization has received increasing attention, once it fulfills the double purpose of waste and material costs reduction [1]. As for rice husk (RH) valorization, particularly, there have been recorded various options such as fuel production, heat/electricity production, agricultural and industrial uses. The latter include constructing materials, chemicals, and adsorbents like biochars [2]. It should be underlined, at this point, that rice husk biochar (RHB) and biochars generally can function as activators of oxidizing agents such as persulfate, besides their use as sorbents [3].

RH makes up at least 20% of the rough rice weight, which means that about  $1.5 \times 10^{11}$  kg of it are produced annually, placing it among the most abundant agricultural product worldwide [4]. Rice cultivation is, also, a significant crop in Greece, given that it is the third largest producer of rice in the European Union (EU) [5]. RH is a lignocellulosic material which consists of 28.6–43.3% cellulose, 22.0–29.7% hemicellulose, 19.2–24.4% lignin and 17–20% ash [6]. The composition of raw biomass can influence the speciation of carbon species in the biochar. Thus, RHB is promising for using in advanced oxidation processes, since biochars from biomass rich in cellulose are known to outperform as persulfate activators those from biomass rich in lignin biomass [7]. Also, its high local availability is an advantage.

Nowadays, biochars are well-known activators of persulfate ions and can be used as catalysts for the oxidation of antibiotics [8], the presence of which in the aquatic environments is a significant problem getting increasing attention due to its correlation with the development of antibiotic resistance [9]. Antimicrobial and especially antibiotic resistance has occurred as a main world health issue of the present century as it threatens the effective prevention and treatment of a wide range of illnesses. The selective increase of antibiotic resistant bacteria in wastewater and freshwater is an important factor contributing to antibiotic resistance, among others [10]. Antibiotics reach the aquatic environment through production plants, urban wastewaters, and livestock. As a result, they have been detected in freshwaters at concentrations ranging from 3 ng/L to 484 µg/L [11]. The higher concentration was detected in Asia in the Xiao river. Sulfamethoxazole (SMX) was measured in concentrations reaching up to 53.828 µg/L in Mozambique, Africa, and at 38.9 µg/L in Kenya [11]. It was the most frequently detected antibiotic and the ninth most detected in terms of concentration in surface waters [12]. SMX contains the sulfonamide group ( $-\text{SO}_2-\text{NH}$ ), an aromatic ring, and an amino group, among others [13]. SMX is slightly acidic with a pKa value of 5.74 [14]. The isoelectric point was reported as 4.5. Usually, it can be found either in neutral form (no-charged) in a wide pH range ( $1.39 < \text{pH} < 5.8$ ) and negative charge in higher pH [15]. The adverse effects of SMX are the common effects of sulfonamides such as rashes, Stevens-Johnson syndrome, anaphylaxis, and angioedema, Photosensitivity and neurologic effects, such as insomnia, and headache. In a recent study it was found that SMX concentrations which affected the microbial growth were higher than those usually found in natural environments [16].

Given that biological treatment has been proven incapable of mineralizing antibiotics completely [17], advanced oxidation processes (AOPs) have arisen, in recent years, as an effective solution to this problem. AOPs include Fenton and Fenton-like reactions, (catalytic) ozonation, photocatalytic oxidation, electrochemical oxidation, and ionizing radiation among others [18]. Adsorption and catalytic oxidation processes, especially when an oxidant is used, can be effective and help to avoid the possible secondary pollution, by decomposing the pollutants completely [19].

Generally, sodium persulfate (SPS) is used as oxidizing agent due to its better characteristics. Specifically, SPS is more stable and easy to transport than  $\text{H}_2\text{O}_2$  solution. Sulfate radicals ( $\text{SO}_4^-$ ) can reach equal or higher redox potential, longer half-life and be more selective compared to hydroxyl ones ( $\text{OH}^\cdot$ ) [20]. Catalytic activation has been proven necessary for the effective production of these radicals. The application of a solid catalyst with low cost, which can activate persulfates is ideal, due to reusability, easy separation, and enhanced stability. Biochars are carbonaceous materials, proved to be able to activate PS for the generation of sulfate radicals and the consequent transformation of organic contaminants [8]. Their advantages include efficiency, abundance, low-cost, and environmental friendliness [21]. They can be produced using any available source of biomass and optimized by altering their production conditions [22]. A recent study demonstrated that biochar could retain its high activity or even improved if it is treated with persulfate anions under intense conditions [23].

There are different possible mechanisms for the activation of persulfate by biochars. Most of the researches propose the radical pathway as the main mechanism although they agree that the singlet oxygen pathway can also followed. Finally, the electron transfer mechanism, where biochar is believed to transfer electrons through the carbon phase to activate the persulfate [13], can be followed.

To the best of our knowledge there are no published articles concerning RHB production to activate persulfate/peroxymonosulfate for the degradation of sulfamethoxazole. The most relevant to our work published articles are the following three, which refer to PS/(peroxymonosulfate) PMS activation by pristine RHB for the degradation of other organic pollutants. However, the effect of pyrolysis temperature on the characteristics and catalytic activity of biochar has not been studied. Shi et al., 2018 [3] produced biochar pyrolyzing RH at 400 °C for 1 h to activate PS for the degradation of p-nitrophenol. Huong

et al., 2020 [24] produced biochar pyrolyzing RH at 450 °C for 4 h to activate PMS for the degradation of tetracycline and bisphenol A. Finally, Li et al., 2020 [25] produced biochar pyrolyzing RH at 700 °C for 2 h to activate PS for the degradation of acid orange 7.

In the present study, we explore the influence of the pyrolysis temperature on the physicochemical characteristics and the activation ability of the biochar from rice husk. For this, four biochars are prepared by pyrolyzing RH at temperature of 400, 550, 700 and 850 °C for 1 h. The prepared biochars were characterized by various physicochemical techniques to determine structural and chemical characteristics and then, were used to activate PS for the oxidative degradation of SMX. The main factors determining the activation and degradation processes were fully examined for the more active biochar.

## 2. Results and Discussion

### 2.1. Physicochemical Characterization of Biochars

Four biochars prepared under four different pyrolysis temperatures are symbolized as RHBX, where X is the pyrolysis temperature. The pyrolysis temperatures were 400, 550, 700 and 850 °C. The prepared samples were characterized with various physicochemical techniques, as mentioned above.

#### 2.1.1. Scanning Electron Microscopy (SEM) and Energy-Dispersive X-ray Spectroscopy (EDX) Analysis

Scanning electron microscopy (SEM) and energy-dispersive X-ray spectroscopy (EDX) analysis are presented in Figures 1 and 2 and Table 1.

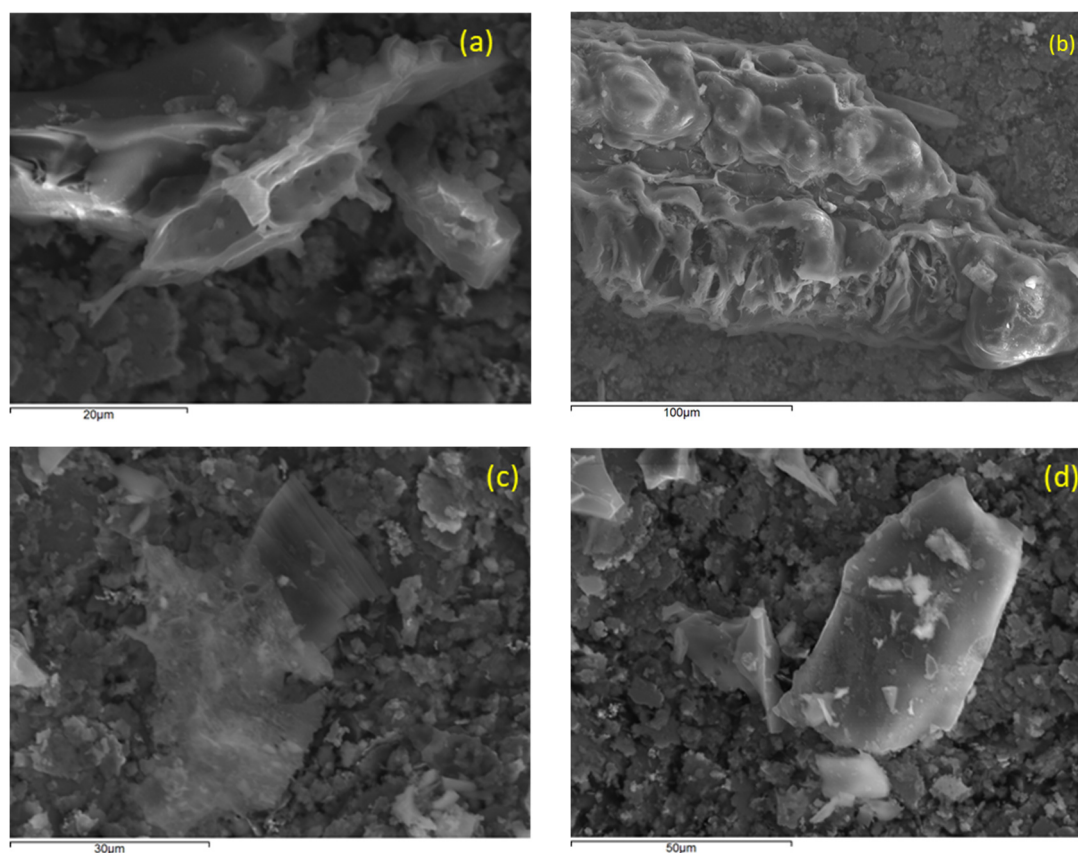


**Figure 1.** Scanning electron microscopy (SEM) images of the prepared biochars; (a) RHB400, (b) RHB550, (c) RHB700 and (d) RHB850.

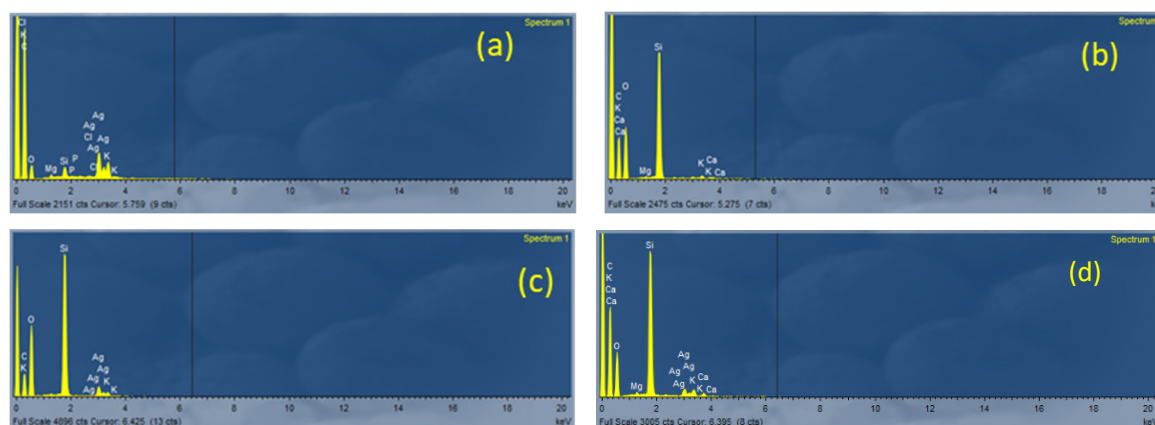


**Figure 2.** Energy-dispersive X-ray spectroscopy (EDX) analysis of the prepared biochars; (a) RHB400, (b) RHB550, (c) RHB700 and (d) RHB850.

**Table 1.** % Atomic concentration of elements of the studied biochars determined by the EDX analysis.

| Element                | RHB400 | RHB550 | RHB700 | RHB850 |
|------------------------|--------|--------|--------|--------|
| C                      | 82.03  | 56.49  | 66.55  | 78.80  |
| O                      | 16.36  | 36.31  | 28.46  | 18.01  |
| Mg                     | 0.19   | 0.08   | 0.035  | 0.16   |
| Si                     | 0.55   | 6.88   | 4.86   | 2.72   |
| P                      | 0.05   | -      | -      | 0.06   |
| Cl                     | 0.09   | -      | -      | 0.08   |
| K                      | 0.71   | 0.16   | 0.09   | 0.13   |
| Ca                     | -      | 0.08   | -      | 0.05   |
| C/O <sup>1</sup> ratio | 5.3    | 2.5    | 3.6    | 6.3    |

<sup>1</sup> The ratio C/O was calculated subtracting O content of the SiO<sub>2</sub> as C/(O-2Si).

As it can be seen from the SEM images, presented in Figure 1, it can be concluded that the organic phase is covered to a higher extent by minerals, with increasing temperature as it was expected, since a higher amount of carbonaceous phase was removed during pyrolysis.

The main minerals in the biochars are the Si, K and Mg. Especially SiO<sub>2</sub> is the main inorganic component due to its abundance in the raw biomass. Indeed, according to the literature the silica content in the ash is about 87–97% [26]. It is interesting that the C/O ratio in the carbonaceous phase increase with the pyrolysis temperature, pointing out that the O species were removed during pyrolysis, especially in higher temperatures.

### 2.1.2. Fourier-Transform Infrared (FTIR) Analysis

The Fourier-transform infrared (FTIR) spectra of the biochars are presented in Figure 3. Generally, there are 5 peaks and their intensity change with the pyrolysis temperature. The peak at about 3400 cm<sup>-1</sup> is due to -OH groups and adsorbed water molecules [27]. This peak is less intense with the temperature, due to the greater extent of burning, pointing out the removal of O containing species during pyrolysis, in accordance with the EDX results. This peak is closely related to the one at 1090 cm<sup>-1</sup>, due to the symmetric C-O stretching. The peak at 1712 cm<sup>-1</sup>, due to C=O groups also depends on the preparation conditions [8]. At higher temperatures this peak can hardly be observed due to the formation of volatile oxygen species and removal of O species. The peak at about 1600 cm<sup>-1</sup> can be attributed to C=C groups, while the absence of any peaks above 3000 cm<sup>-1</sup>, due to the -C-H stretching, is an evidence of the absence of aromatic H, pointing out an aromatic phase poor in hydrogen [28,29]. Finally, the low intensity of the peaks in the region of 1000–1800 cm<sup>-1</sup> for the RHB700 and RHB850 is characteristic of the heterogeneity of these biochars, probably due to the high content of minerals [30].

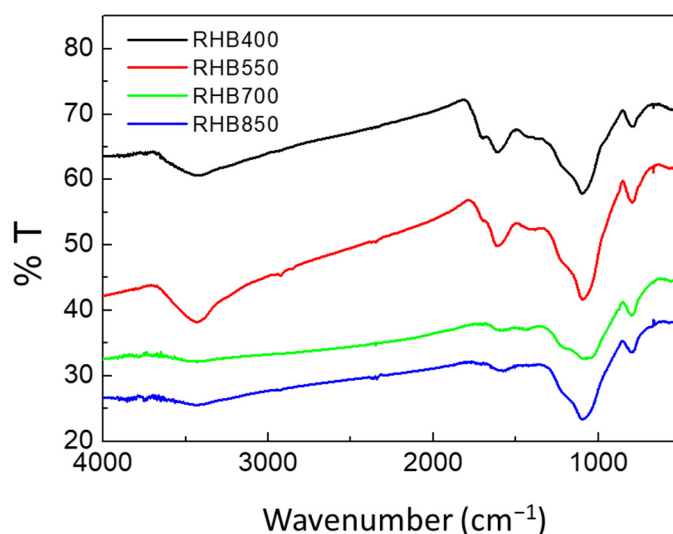


**Figure 3.** Fourier-transform infrared (FTIR) spectra of the biochars studied.

### 2.1.3. Specific Surface Area (SSA) Determination

The values of SSA were determined with the BET method from the adsorption data of  $N_2$  at liquid  $N_2$  temperature and the micropores surface area was calculated with the t-plot method. The microporosity is higher for the samples prepared in 700 and 800 °C. The values are presented in Table 2 and it is also supported from the high values of adsorbed  $N_2$  in low P/Po, an evidence for the microporosity [31–34]. As can be seen, the pyrolysis temperature increases the SSA values and the micropores surface area. Pyrolysis temperatures up to 550 °C are capable of forming biochars with high surface area. The increase of pyrolysis temperature from 550 to 700 °C influences significantly only the micropores and not the total SSA. On the other hand, the biochar with the higher value of SSA is the RHB850, resulting to SSA of  $334 \text{ m}^2\text{g}^{-1}$ , with high microporosity. The total pore volume appears to be stable with pyrolysis temperature up to 550 °C [22].

**Table 2.** Physicochemical characteristics of the biochars studied.

| Sample | SSA ( $\text{m}^2\text{g}^{-1}$ ) | Micropores SSA ( $\text{m}^2\text{g}^{-1}$ ) | Vpore (mL) | % TGA Minerals | pzc |
|--------|-----------------------------------|--|------------|----------------|-----|
| RHB400 | 44.5                              | 28.7   | 0.08       | 34             | 3.6 |
| RHB550 | 262                               | 65   | 0.15       | 42             | 6.3 |
| RHB700 | 231                               | 177  | 0.15       | 47             | 7.4 |
| RHB850 | 334                               | 231  | 0.18       | 57             | 7.8 |

### 2.1.4. X-ray Diffraction (XRD) Analysis

The X-ray diffraction (XRD) patterns of the biochars studied are presented in Figure 4. There are two broad peaks, characteristic of amorphous carbon forms, centered at about  $22^\circ$  and  $43.3^\circ$ . The first peak can be assigned to (002), while the second to (100) crystal planes of hard carbon in lignocellulose form [30,35].

The second peak is only present at the two biochars prepared in high pyrolysis temperature. This peak is due to structures where the C has  $sp^2$  hybridization since it represents the graphitic structure, which improves electrical conductivity [36,37].

The first peak indicates parallel accumulation of graphite sheets. The pyrolysis temperature is one of the factors for the well formation of these two peaks. Finally, the absence of any sharp peaks in XRD patterns denotes that there are no crystalline inorganic phases pointing out that the  $SiO_2$  present is amorphous.

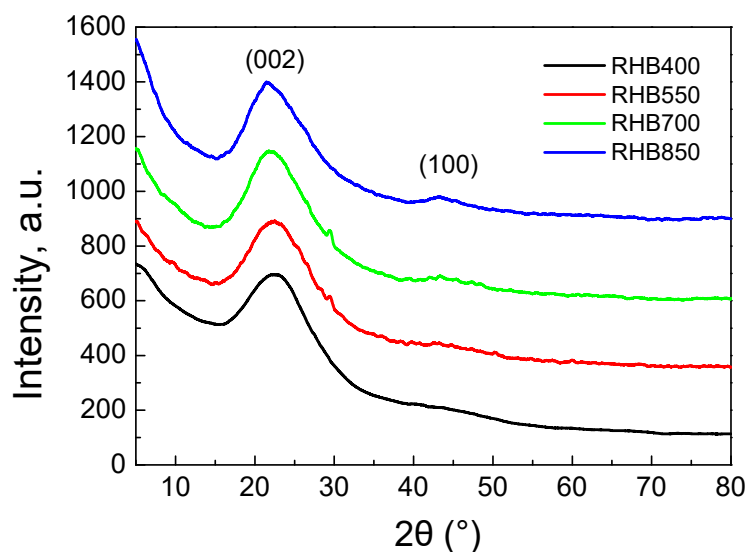


Figure 4. X-ray diffraction (XRD) patterns of the studied biochars.

#### 2.1.5. Thermogravimetric Analysis (TGA)

Thermogravimetric analysis (TGA) was performed under air flow of  $20 \text{ mL min}^{-1}$  with a heat rate of  $10 \text{ °C min}^{-1}$  and presented in Figure 5. Under these conditions the carbonaceous phase is expected to fully burn, and the residuals can be attributed to minerals and the nonvolatile inorganic phase.

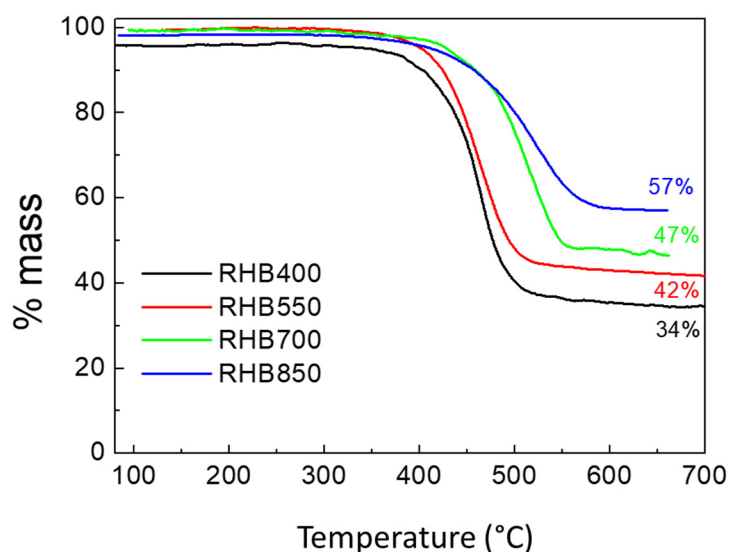


Figure 5. Thermogravimetric analysis (TGA) curves, under air atmosphere for the biochars studied.

At the beginning of the thermal treatment an isothermal step for 1 min in  $80 \text{ °C}$  was applied, to remove the adsorbed water. For all the biochars there is a small mass loss, due to adsorbed water, which is higher for the RHB400. During thermal treatment a sharp decrease in the mass was observed for all the samples, resulting in the burn of the organic phase and the removal of C. Interestingly, the temperature where the decomposition occurs increases with the pyrolysis temperature. This clearly shows that burning the carbonaceous phase requires a higher amount of heat since higher pyrolysis temperatures transform the carbonaceous phase to hard carbon. This was also observed in different biochars after treatment with acid or base solution, where the carbonaceous phase was different after treatment and exhibits differences in the burning temperature [33]. The amount of the minerals can be estimated by the mass left in TGA run. The RHB850 sample has more than

half of its weight minerals, while the RHB400 has 34%. Since higher pyrolysis temperatures results in increased removal of organic phase this is expected. The mass of the minerals left after TGA run is reported in Table 2.

#### 2.1.6. Potentiometric Mass Titrations (PMT)

The determination of point of zero charge, pzc of the samples was performed with the potentiometric mass titration technique [38]. According to this the pzc of the solid is the section point of one (or more) titration curve of the suspension with the corresponding curve of the solution (blank solution, a solution of the same indifferent electrolyte without biochar). The pH of this section point is the point of zero charge, pzc, of the biochar. In pH values lower than the pzc, the surface of the biochar is positively charged, while in higher values the surface develops negative charge due to the deprotonation of the surface sites. Usually, the reported values have been determined using microelectrophoresis. This method does not provide the pzc value but the iep, the isoelectric point. This is the pH of which the zeta potential is equal to zero, and not the surface charge. These two values are the same only if no specific adsorption occur. Otherwise the values are different. When a specific adsorption occurs the pzc and iep shift to different direction. For example when a cation is adsorbed then the pzc shift to lower values and iep to higher [39]. The opposite is valid for the anion adsorption.

The potentiometric titration curves of the biochars studied are presented in Figure 6. The values of pzc are presented in Table 2. A rise in the pyrolysis temperature increases the pzc of the biochar. This is due to the removal of the O surface species, phenolic and carboxy groups, which, in general, present weak acidic properties.

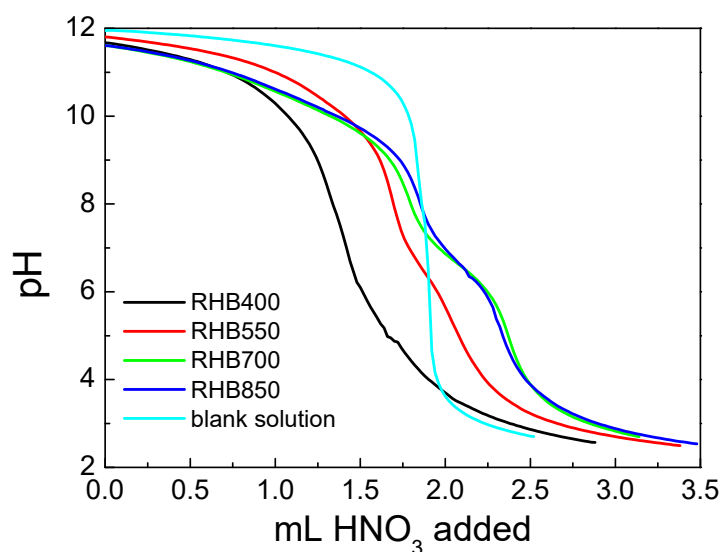


**Figure 6.** Potentiometric titration curves for the rice husk (RH) biochars and the blank solution.

The physicochemical characterization clearly showed that the biochar can be successfully formed in temperatures of 400 °C and higher. The pyrolysis temperature significantly affects the characteristics of the biochar, while its rise significantly increases the SSA. The increment of SSA starts first in the mesoporous and macroporous regions. Pyrolysis temperatures above 550 °C is required for the increment of the microporous area as it was found that RHB550 and RHB700 samples possess almost the same SSA, but there is a significant difference in the value of the micropores surface area. Higher temperatures also transform the carbon phase to a harder phase with fewer oxygen groups and higher graphitic character with improved electrical conductivity. The removal of oxygen groups reduces the surface acidity shifting the pzc values from 3.6 to 7.8.

## 2.2. Oxidative Degradation of Sulfamethoxazole (SMX)

### 2.2.1. Effect of Pyrolysis Temperature

As can be observed in Figure 7, the efficiency of SMX degradation is defined to a great extent by the kind of biochar used in the process, and thus from pyrolysis temperature. The general tendency is that catalytic reactivity increases as pyrolysis temperature increases, in the range that was examined (400–850 °C). Biochars produced by pyrolysis of RH up to 400 °C or 550 °C showed insufficient activation of SPS, reaching 19% and 29% removal of the pollutant, respectively, after 120 min, when using 100 mg/L biochar and 500 mg/L SPS in ultrapure water (UPW) and inherent pH. On the contrary, biochars produced by pyrolysis of RH up to 700 °C or 850 °C showed interesting results, reaching 55% and 96% SMX removal, respectively, after 120 min. It is to be noted that SMX removal surpassed 90% after 60 min in the case of RHB 850.

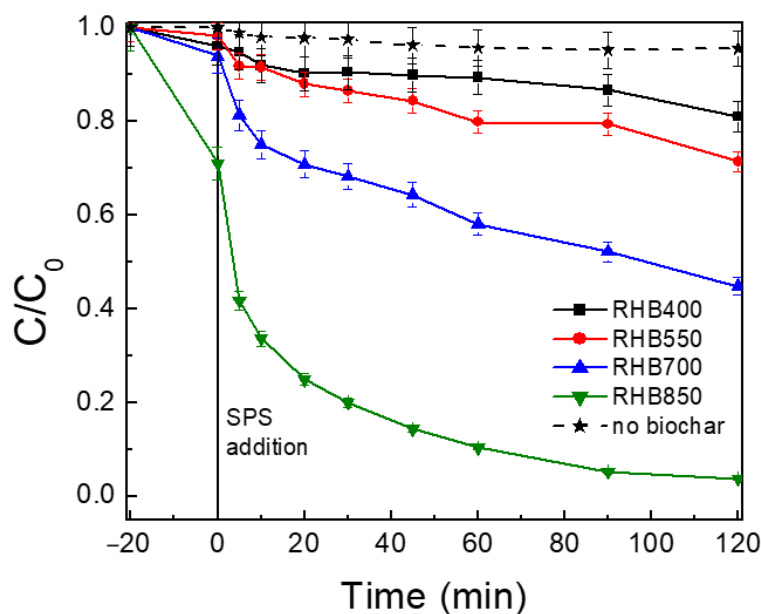


**Figure 7.** Effect of pyrolysis temperature on 500 µg/L sulfamethoxazole (SMX) degradation with 100 mg/L biochar and 500 mg/L sodium persulfate (SPS) in ultrapure water (UPW) and inherent pH and temperature. SPS was added at  $t = 0$ .

The adsorption of SMX on the biochars is also influenced by pyrolysis temperature as can be seen in Figure 8. For pyrolysis temperatures up to 700 °C, no significant differences can be noted, achieving 8–12% removal of the pollutant after 120 min, when using 100 mg/L biochar in UPW and inherent pH. On the other hand, SMX adsorption on RHB 850 is quite impressive reaching 55% after 120 min. RHB 850 can be an excellent sorbent of hydrophobic organic compounds like SMX. This is due to its high surface area, fewer functional groups, and lower surface charge. These results agree with the respective for biochars prepared using other kinds of biomass [22]. Hu et al., 2008 [40] had concluded that the increase of pyrolysis temperature results in final biochar with fewer OH, C–H and C–O groups that mainly consists of aromatic polymers of carbon atoms. A decrease in H/C ratio, at higher pyrolysis temperatures, indicates an increase in BC's aromaticity, which can cause strong electron giving-accepting effects on aromatic pollutants through conjugated  $\pi$ -electron structure [41]. It has also been reported that biochars produced by pyrolysis for 1 h present a higher level of persistent free radicals, which are able to activate persulfate, as the pyrolysis temperature rises [21].

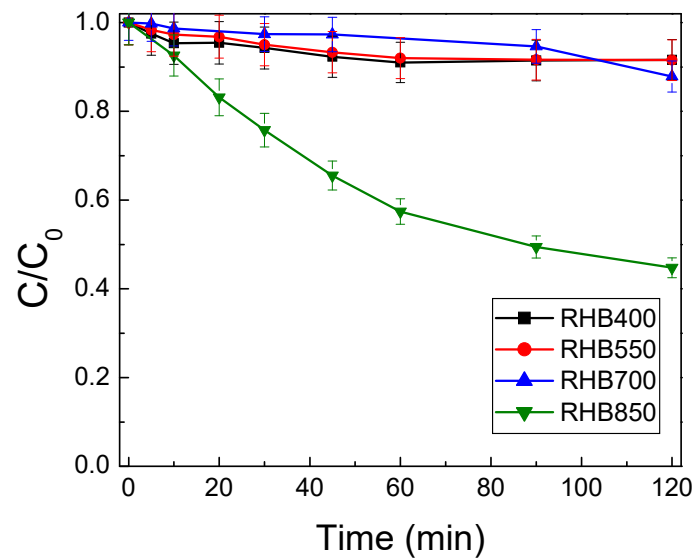


**Figure 8.** Adsorption of 500 µg/L SMX onto 100 mg/L RHB samples in UPW and pH = 5.6.

### 2.2.2. Effect of Sodium Persulfate (SPS), Biochar and SMX Concentration

The influence of SPS concentration is presented in Figure 9. With no SPS the removal of SMX is due to adsorption alone. The adsorption is significant and about 55% after 120 min. The addition of SPS increases the degradation of SMX and it was found that after 60 min almost complete removal of SMX occurs with 500 mg L<sup>-1</sup> SPS. The logarithms of  $C/C_0$ , shown in Figure 9 have a very good linear correlation with time, confirming the pseudo-first order kinetic. More details about the kinetic analysis can be found in [27]. The apparent kinetic constants ( $k_{app}$ ) computed from the slopes of the respective tendency lines, show an increase with the SPS concentration up to 500 mg/L and a plateau above this concentration. This is an evidence that SPS activation occurs on the surface sites of the biochar.

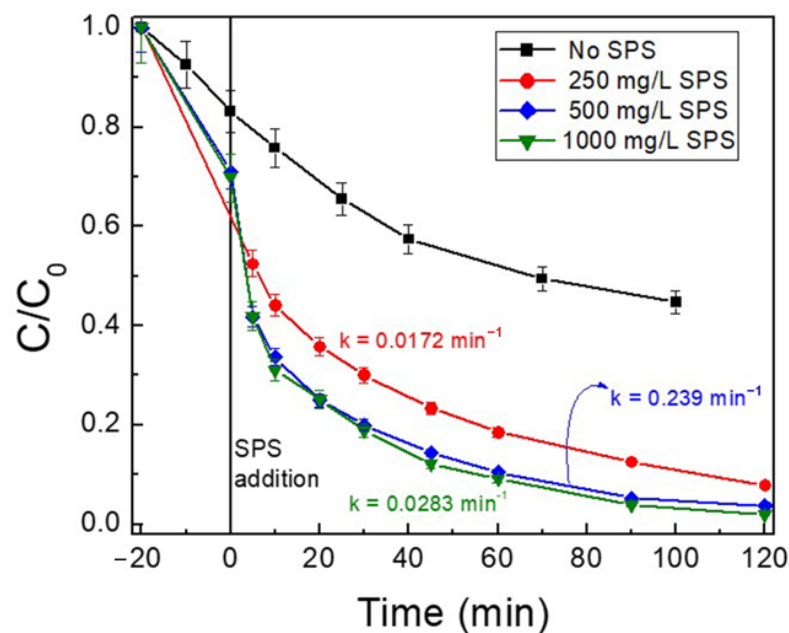


**Figure 9.** Effect of SPS concentration on 500 µg/L SMX degradation with 100 mg/L biochar (RHB 850) in UPW and pH = 5.6.

The influence of the biochar amount is presented in Figure 10, while  $k_{app}$  values were computed from the degradation data, assuming pseudo-first order kinetic.

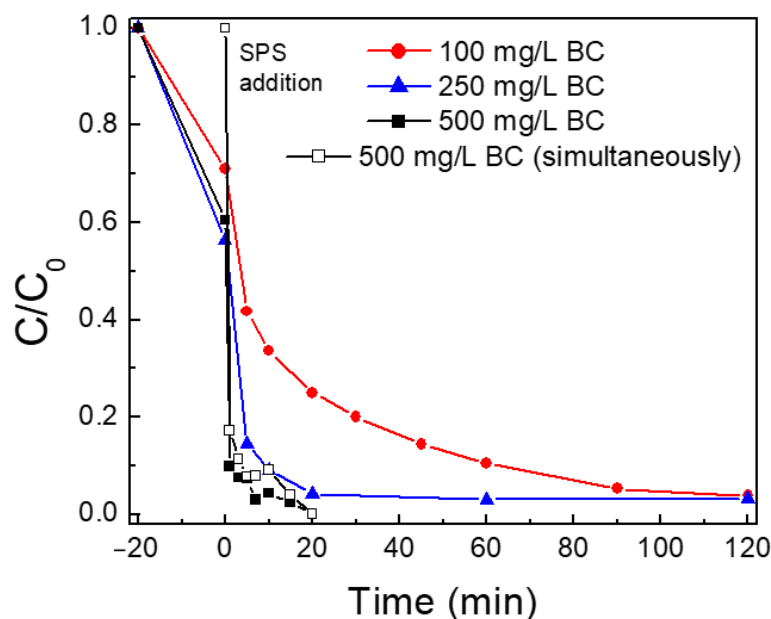


**Figure 10.** Effect of biochar (RHB 850) concentration on 500 µg/L SMX degradation with 500 mg/L SPS in UPW and pH = 5.6.

For RHB850, the  $k_{app}$  values were computed equal to  $2.39 \times 10^{-2}$  (100 mg/L biochar)  $4.53 \times 10^{-2}$  (200 mg/L biochar) and  $1.42 \times 10^{-1} \text{ min}^{-1}$  (500 mg/L biochar), i.e., a five-fold increase in biochar concentration resulted in a six-fold increase in the rate constant. These results agree with the use of biochar from olive stones as catalyst [27]. Interestingly, the application of 500 mg/L RHB850 can almost eliminate the SMX in a very short treatment time (about 10 min). The main process for the removal of SMX is the degradation process since the same results were also obtained in the case that SPS and RHB850 were simultaneously added to the SMX solution. In this case there was a sharp decrease of the SMX concentration of 83% in the first minute, while more than 92% of the SMX had been removed after 5 min. This was in agreement with the kinetics curves of the activation of SPS [23]. These curves show that only a small portion of SPS consumed by the biochar with the first 10 min and then the concentration of SPS remains constant with time [23].

Figure 11 presents the effect of initial SMX concentration. Concentrations from 500–2000 µg/L were selected. The increase of SMX concentration results in lower degradation of SMX. This, also, can be seen from the  $k_{app}$  values. These values calculated with the pseudo first order kinetic approach and the values were found to depend with the SMX concentration, suggesting that the reaction is not truly first order. The  $k_{app}$  values were  $2.39 \times 10^{-2}$ ,  $1.28 \times 10^{-2}$ , and  $6.6 \times 10^{-3} \text{ min}^{-1}$  at 500, 1000 and 2000 µg/L SMX, respectively. The oxidation rate is influenced by the absorbed SMX for a given set of experimental conditions, since the formation of the free radical can be consider constant. With increasing SMX concentration the formation of radical through activation of SPS is hindered and thus the oxidation is slower.

The results are promising for the use of RH biochar as a catalyst for persulfate to oxidize SMX, given that the application of 500 mg/L RHB850 and 500 mg/L SPS can achieve almost complete removal of 500 µg/L SMX in 5 min under inherent conditions.

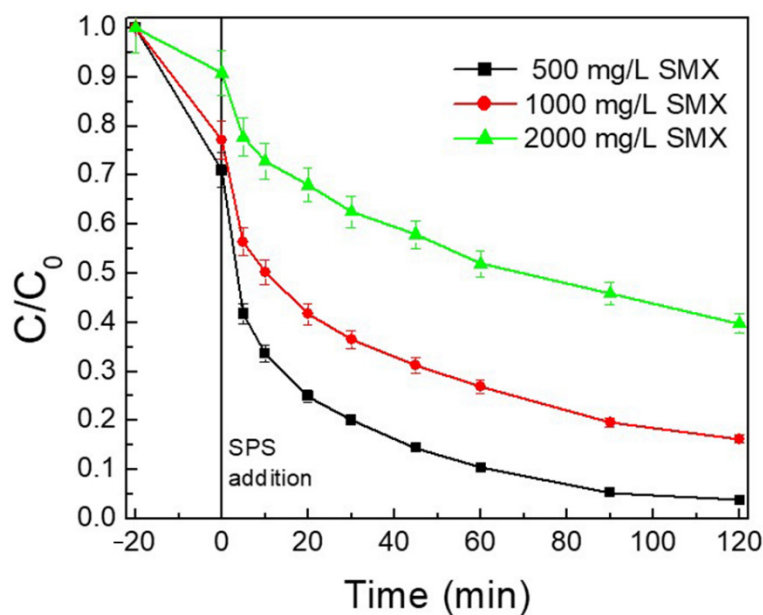


**Figure 11.** Effect of initial SMX concentration on its degradation with 100 mg/L biochar (RHB 850) and 500 mg/L SPS in UPW and pH = 5.6.

In particular, RHB850 seems to activate SPS effectively compared to other pristine biochars derived from different agro-industrial residuals, which were prepared before by our research group. Indeed, it exhibited about the same reaction rate constant ( $2.91 \times 10^{-2} \text{ min}^{-1}$ ) with the biochar from spent malt rootlets [8] for the same experimental conditions (250  $\mu\text{g/L}$  SMX, 90 mg/L BC, 250 mg/L SPS). It performed 2.5 times more efficiently ( $k_{app} = 2.83 \times 10^{-2} \text{ min}^{-1}$ ) than the biochar from spent coffee grounds [13] for the same experimental conditions (500  $\mu\text{g/L}$  SMX, 100 mg/L BC, 1000 mg/L SPS), while it was found to be 4.8 more efficient than the biochar from olive stones [29] for the same experimental conditions (500  $\mu\text{g/L}$  SMX, 200 mg/L BC, 500 mg/L SPS).

On the other hand, treatment of the biochars showed a noteworthy enhancement of SMX degradation. For example, larger quantities of SMX were able to be oxidized where graphitization, and N-doping in some of the cases, of the catalyst took place, using ammonium nitrate [42], the N-containing protein in *Spirulina* [43], potassium carbonate [44], potassium ferrate [45], ammonium ferric citrate [46], or urea [47]. These data indicate possible future perspectives for further studies, for example degradation of higher pollutant concentrations [48], or mixtures of pharmaceuticals as they existed in environmental samples. Nevertheless, a possible modification of biochar should be considered holistically and from the circular economy's perspective to have a comprehensive assessment of the environmental footprint of the proposed process.

### 2.2.3. The Water Matrix Effect

The influence of water matrix was explored using bottled water (BW) and secondary treated wastewater (WW) instead of UPW. The water matrix effect is depicted in Figure 12. In all cases, the SMX oxidation is slower in real matrices compared to ultra-pure water; for example the 86% conversion after 45 min in UPW decreases to 63% and 32% in BW and WW, respectively, due to inherent presence of various inorganic and organic, non-target species in real matrices and their competition with SMX for the oxidizing species and the catalyst surface area. A possible solution to the deceleration of the process in WW could be the increase of BC dose: the experiment was repeated using 500 mg/L of BC resulting in complete degradation of the target pollutant within the first hour.

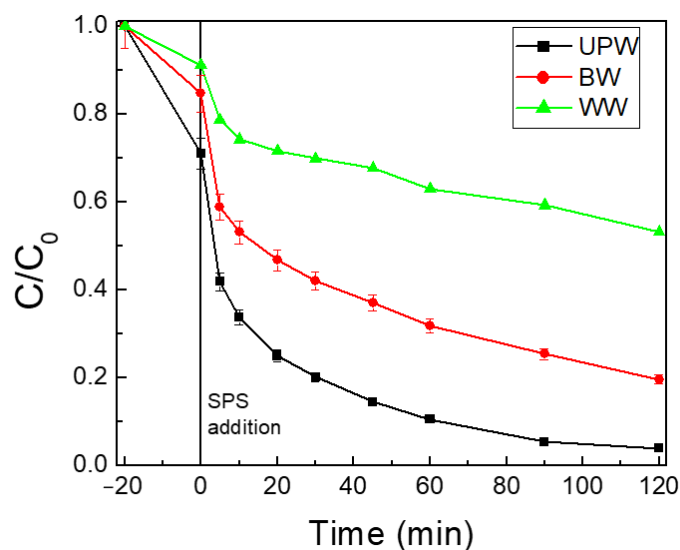


**Figure 12.** Effect of water matrix on 500 mg/L SMX degradation with 100 mg/L biochar (RHB 850) and 500 mg/L SPS at pH = 5.6.

We tried to find out the components that have detrimental effect on the SMX degradation experiments using spiked solutions with various non-target species, namely, bicarbonate, chloride and humic acid. To compare the results we used the  $k_{app}$  values and the results are summarized in Figure 13. The most severe inhibition was from bicarbonate ions leading to only 24% removal compared to the experiment without bicarbonates. This can be attributed either to scavenging action of bicarbonates or to the competitive adsorption of these anions on the biochar surface. The latter can influence the electron transfer pathway since it is known that the first step in this pathway is the adsorption of persulfates on the biochar surface [49].

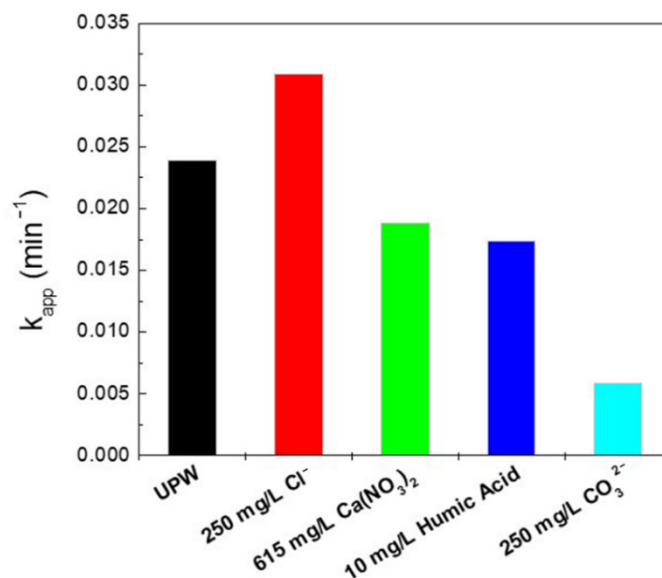


**Figure 13.** Effect of the addition of bicarbonates ( $\text{CO}_3^{2-}$ ), chloride, calcium nitrate ( $\text{Ca}(\text{NO}_3)_2$ ) or humic acid on 500  $\mu\text{g}/\text{L}$  SMX degradation with 100 mg/L biochar (RHB 850) and 500 mg/L SPS at inherent pH.

Calcium nitrate at multiple concentration (double for the calcium cation), compared to the values usually found in bottle waters, had an intermediate impeding effect on the process. Chlorides at multiple concentration, compared to the environmental one, is

slightly enhancing. The above are in accordance with degradation in BW that contains, among others, calcium, nitric, bicarbonate and chloride ions.

The effect of humic acid is not very significant, at a concentration relevant to that of wastewater.

#### 2.2.4. Influence of Initial pH on SMX Adsorption and Degradation

Solution pH seems to be one of the most important factors, which affects SMX adsorption and degradation. The removal of SMX at different initial pH values is presented in Figure 14 either by adsorption or oxidation. Concerning the adsorption process, it is significantly affected by pH, pointing out that the  $\pi$ - $\pi$  interactions are not the only factor that rules the adsorption process, but electrostatic interactions also occur. These interactions originate from the combined result of the surface charge of the RHB850 and the isoelectric point of SMX. The pzc value of the RHB850 is 7.8, a value close to neutral, which means that the surface groups do not have significant acidic or basic properties. On the other hand, SMX has positive charge only under highly acidic conditions ( $\text{pH} < 1.4$ ) and negative charge at  $\text{pH} > 6$ . [14,15]. Under basic conditions the RHB surface deprotonates to develop negative charge and this deprotonation releases  $\text{H}^+$  in the solution resulting in lower pH values and the shift from 9.9 to 6.4. Under this pH the SMX is negatively charged and the adsorption is not favorable. At inherent pH the mechanism is different. The biochar surface is slightly positive and the neutral/negative form of SMX can be adsorbed. The adsorption of the SMX species (open symbols) increases the pzc value and as a result the pH is slightly increased too. Finally, under acidic conditions the surface of RHB850 is positively charged making easy the adsorption of the neutral form of the SMX, resulting in higher adsorption. This behavior agrees with previously reported results [13,27]. The addition of 500 mg/L SPS changes the process (solid symbols). During oxidation the acidity of the solution increases even when initial conditions are basic or neutral, due to the production of  $\text{HSO}_4^-$ . This pH change is evidence of the activation of SPS and the formation of sulfate radicals. This radical formation is accompanied by the production of  $\text{HSO}_4^-$  as a side product. Therefore, the distribution of the different reactive species is pH-dependent. It is well documented that sulfate radicals have a lower oxidation potential than hydroxyl radicals. On the other hand, they have a longer lifespan, thus increasing the likelihood of reacting with SMX on the catalyst surface and exhibit also greater selectivity. However, progressive decrease of pH results in less pronounced differences after 120 min of the process. In addition, the differences are more significant in shorter time intervals, up to 40 min, where the pH has not reached the minimum value yet. Therefore, the optimal conditions are acidic, but, due to the generation of  $\text{H}^+$  during oxidation, the system may function without pH regulation.

#### 2.2.5. The Role of Radical Scavengers

The addition of methanol or *t*-butanol (0.12 mol/L), well known radical scavengers, were used to check the contribution of free radicals in the degradation process. Methanol reacts with both sulfate and hydroxyl radicals at similar rates, while *t*-butanol reacts preferentially with hydroxyl radicals [47,50]. Also, the addition of sodium azide, a well-known scavenging factor of the singlet oxygen reactions, was tried [51]. As can be seen in Figure 15, SMX degradation is slightly impeded by either alcohol, but strongly decelerated by sodium azide, the  $k_{app}$  decreases from  $2.39 \times 10^{-2} \text{ min}^{-1}$  for UPW to  $1.62 \times 10^{-2}$ ,  $1.54 \times 10^{-2}$  and  $8.6 \times 10^{-3} \text{ min}^{-1}$  for methanol, *t*-butanol and sodium azide, respectively.

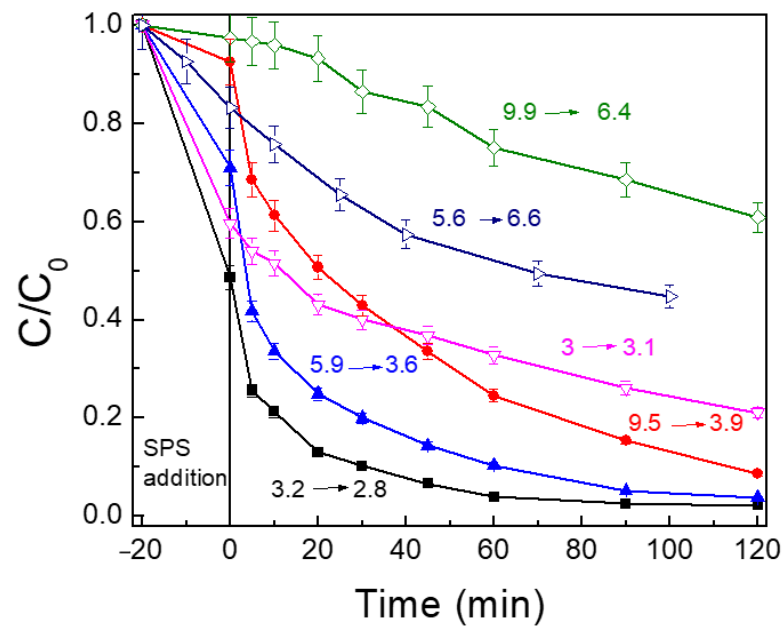


**Figure 14.** Effect of initial pH on 500  $\mu\text{g/L}$  SMX adsorption (open symbols, no SPS) and degradation (solid symbols, 500 mg/L SPS) with 100 mg/L biochar (RHB 850) in UPW. Initial and final pH values are noted on the graph.

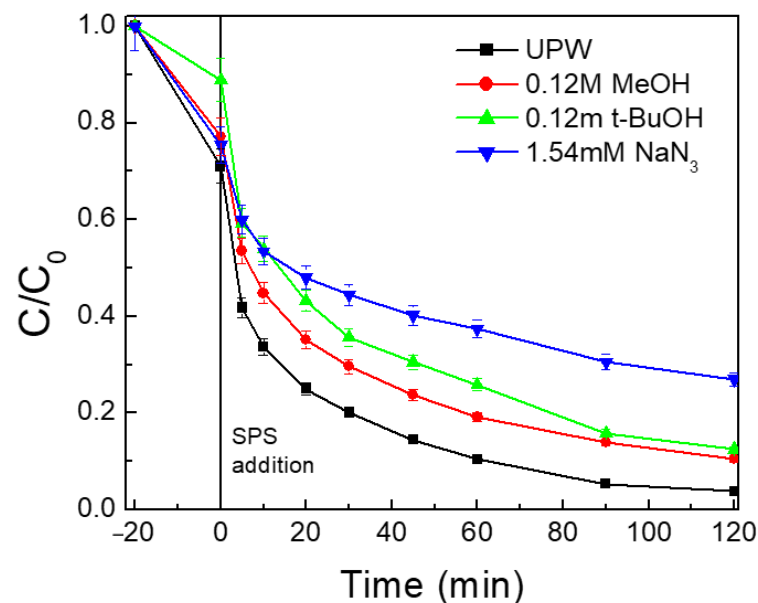


**Figure 15.** Effect of alcohols and sodium azide on 500  $\mu\text{g/L}$  SMX degradation with 100 mg/L biochar (RHB 850) and 500 mg/L SPS in UPW and inherent pH.

The influence of the alcohol addition is more complicated since it alters also the extent of SMX adsorption on the biochar surface, i.e., 21% for methanol and 62% for t-butanol. The lower adsorption of SMX can partially explain the lower oxidation rates, since oxidation mainly occur on the surface. Since t-butanol has greater affinity for hydroxyl radicals than methanol [52] it can be hypothesized that hydroxyl radicals outcompete sulfate radicals, to an extent. At the same time, the evident inhibition caused when sodium azide is added indicates the significant contribution of the singlet oxygen pathway to SMX destruction. This behavior has also been reported elsewhere [13,53]. It seems that biochar surface groups are crucial for persulfate activation. The degradation may follow different pathways where

radicals formed on the biochar surface and non-radical pathways can be followed [54]. According to this degradation may occur not only through  $\text{SO}_4^-$  and  $\text{HO}\cdot$  radicals, but also through singlet oxygen  $^1\text{O}_2$ , and electron transfer routes. Since methanol or t-butanol have a limited inhibition effect electron transfer may be the main pathway in contrast with the cases that transition metal ion is supported on the carbonaceous phase where the predominant mechanism is the radical oxidation [55]. Yin et al., 2019 [47] have referred to singlet oxygen as the predominant mechanism of PS activation for the degradation of SMX.

### 2.3. Physicochemical Characteristics of Biochar and Oxidation Activity

The physicochemical characteristics of biochar play an essential role in the oxidation process. The high surface area of the RHB850 is the first characteristic of the biochar that is beneficial for the degradation. As expected, high removal rates were achieved in the cases where the adsorption of SMX is increased. Indeed, the adsorption of SMX and probably SPS is the first step in the oxidation. This behavior can be seen in several experiments like the influence of pH presented in Figure 14. Under acidic conditions adsorption and degradation are favored, pointing out the adsorption of SMX and the activation of SPS which are enhanced by the pH decrease. Also, the presence of t-butanol (Figure 15) significantly affects the adsorption of SMX and thus the degradation process. On the other hand, the surface area is not the only factor affecting the degradation process. Surface groups and the carbon phase are also significant. The presence of C=O groups are not favorable for the degradation process and the activation of SPS is in contrast with the presence of C–O groups [23], while the graphitic carbon form increases the activity. High pyrolysis temperatures can regulate the population of oxygen surface groups due to the removal of higher amounts of O and the subsequent increase of the C/O ratio. XRD and TGA results reveal that the carbon phase is transformed to a “harder” form of carbon with higher conductivity and thus activity in the electron transfer pathway. This is in accordance with the inhibition of  $\text{NaN}_3$  presented in Figure 15. Thus, it can be concluded that a good potential biochar for the oxidation of organic compounds in water should have high surface area, tunable microporosity and pore volume, significant amount of not fully oxidized C–O groups and high amounts of graphitic carbon. In addition to the above characteristics, the RHB850 can be produced from waste bio-mass, increasing the sustainability of the process, making it an excellent and attractive prospect for the degradation of SMX.

## 3. Materials and Methods

### 3.1. Production of Biochar

RH was procured from the rice processing factory of Agrino S.A., Agrinio, which is in Western Greece. A pre-weight RH quantity was placed into a ceramic vessel sealed with a ceramic cap, thus retaining a limited oxygen atmosphere, about 20% of the required  $\text{O}_2$  for full oxidation. The vessel was placed in a gradient temperature furnace (LH 60/12, Nabertherm GmbH, (LH 60/12, Nabertherm GmbH, Lilienthal, Germany) reaching a temperature of 400 °C and pyrolyzed for 1 h at the selected temperature. The procedure was repeated for three more pyrolysis temperatures of 550 °C, 700 °C and 850 °C. Then, the biochars were collected and sieved mechanically to get fractions of different particle sizes. Finally, the fraction of particle size <150  $\mu\text{m}$  was chosen and used in the activation processes.

### 3.2. Chemical Compounds

Sulfamethoxazole (SMX,  $\text{C}_{10}\text{H}_{11}\text{N}_3\text{O}_3\text{S}$ , 99+%, CAS number: 723-46-6), sodium persulfate (SPS,  $\text{Na}_2\text{S}_2\text{O}_8$ , 99+%, CAS number: 7775-27-1), sodium chloride (NaCl, 99.8%, CAS number: 7647-14-5), and sodium bicarbonate ( $\text{NaHCO}_3$ , 99.7%, CAS number: 144-55-8) were obtained from Sigma-Aldrich (St. Louis, MO, USA.). Acetonitrile (99.9 wt%), humic acid (HA, technical grade), sodium hydroxide (98 wt%), methanol (99.9%), t-butanol (99%) and sulphuric acid (95 wt%) were also purchased from Sigma Aldrich. Sodium azide ( $\text{NaN}_3$ , 99+%, CAS number: 26628-22-8) was purchased from Merck (Merck KGaA,

Darmstadt, Germany). Calcium nitrate hydrate ( $\text{Ca}(\text{NO}_3)_2 \cdot \text{H}_2\text{O}$ , 99.9%, CAS number: 35054-52-5) was purchased from Fluka (Loughborough, England).

### 3.3. Experimental Procedure

Degradation experiments were conducted in a 150 mL pyrex vessel, open to the atmosphere. The desired SMX concentration was prepared with dilution of a stock SMX solution (50 mg/L) at a total initial volume of 120 mL.

More details about the catalytic runs can be found in literature [13]. In most experiments, UPW was the water matrix, while some experiments were also performed in bottled water (BW, pH = 7.5, 356  $\mu\text{S}/\text{cm}$  conductivity, 237.9238 mg/L  $\text{HCO}_3^-$ , 7.92 mg/L  $\text{SO}_4^{2-}$ , 3.84 mg/L  $\text{Cl}^-$ ) or secondary treated wastewater (WW, pH = 8.3, 4 mg/L total organic carbon, 9 mg/L total suspended solids, 14 mg/L chemical oxygen demand, 1.826 mS/cm conductivity, 66 mg/L  $\text{SO}_4^{2-}$ ).

### 3.4. Samples Analysis

A volume of 1.2 mL was withdrawn each sampling time and were analyzed via liquid chromatography. More information about the mobile phase and the absorbance peak can be found in Lykoudi et al., 2020 [13]. The limits of SMX detection and quantification were 6.9 and 20.7  $\mu\text{g}/\text{L}$ , respectively [56].

### 3.5. Physicochemical Characterization of the Biochars

The physicochemical characterization of the prepared biochars was performed according to the literature [13,27,33,57].

## 4. Conclusions

The main conclusions of the present study are summarized as follows:

- (i) Biochars for rice husk can be activate SPS for the oxidation of SMX. High pyrolysis temperature can contribute to biochar with the desired physicochemical characteristics and high SPS activation ability, leading to high SMX oxidation values.
- (ii) High biochar and moderate SPS concentration favor the SMX degradation. The process follows a pseudo-first order kinetic rate and the initial solution pH affects the adsorption process but it is not a crucial factor for the degradation process.
- (iii) Degradation in real matrices (BW and WW) occurs slower than in ultra-pure water; bicarbonate ions have a detrimental effect on the degradation. Conversely, humic acid (a representative of natural organic matter) has no remarkable effect on degradation.
- (iv) The alcohol scavenging action towards radicals is limited, contrary to that of sodium azide. This indicates that degradation may occur on the surface by both radical and non-radical (singlet oxygen, electron transfer) pathways and adsorption of SMX plays an important role in the degradation process. At the same time, the oxidation in the bulk solution is limited.
- (v) Almost complete SMX removal can be achieved with RHB850 concentration of 500 mg/L within 5 min for UPW and within an hour for WW.

**Author Contributions:** E.A.: Investigation, Formal Analysis and Writing, Z.F.: Reviewing, J.V.: Investigation, Writing—Reviewing and Editing, I.D.M.: Resources and Investigation, D.M.: Conceptualization, Funding acquisition and Editing. All authors have read and agreed to the published version of the manuscript.

**Funding:** E.A. and D.M. acknowledge support of this work by the project “Biochars from Valorized Biomass, Oxidants, Hazardous and Emerging Micro-Pollutants and the Water Matrix: Does their Interplay Affect Notably Treatment Performance?” funded by the Hellenic Foundation for Research and Innovation (H.F.R.I.) under the “First Call for H.F.R.I. Research Projects to support Faculty members and Researchers and the procurement of high-cost research equipment grant” (Project Number: 81080).

**Acknowledgments:** Authors are thankful to Katerina Govatsi, University of Patras, School of Natural Sciences, Laboratory of Electron Microscopy and Microanalysis (LEMM) for the SEM measurements and would also like to thank Agrino S.A. for the procurement of rice husk.

**Conflicts of Interest:** The authors declare no conflict of interest.

### Abbreviations

|      |                               |
|------|-------------------------------|
| SMX  | sulfamethoxazole              |
| SPS  | sodium persulfate             |
| RHB  | rice husk biochar             |
| UPW  | ultrapure water               |
| BW   | bottled water                 |
| WW   | wastewater                    |
| SSA  | Specific surface area         |
| XRD  | X-ray diffraction             |
| FTIR | Fourier transform infrared    |
| SEM  | scanning electron microscopy  |
| TGA  | Thermogravimetric analysis    |
| PZC  | Point of zero charge          |
| PMT  | potentiometric mass titration |

### References

1. Tongcumpou, C.; Usapein, P.; Tuntiwattanapun, N. Complete utilization of wet spent coffee grounds waste as a novel feedstock for antioxidant, biodiesel, and bio-char production. *Ind. Crop. Prod.* **2019**, *138*, 111484. [[CrossRef](#)]
2. Goodman, B.A. Utilization of waste straw and husks from rice production: A review. *J. Bioresour. Bioprod.* **2020**, *5*, 143–162. [[CrossRef](#)]
3. Shi, C.; Li, Y.; Feng, H.; Jia, S.; Xue, R.; Li, G.; Wang, G. Removal of p-Nitrophenol using persulfate activated by biochars prepared from different biomass materials. *Chem. Res. Chin. Univ.* **2018**, *34*, 39–43. [[CrossRef](#)]
4. Singh Aulakh, D.; Singh, J.; Kumar, S. The effect of utilizing rice husk ash on some properties of concrete-A review. *Curr. World Environ.* **2018**, *13*, 224–231. [[CrossRef](#)]
5. Kraehmer, H.; Thomas, C.; Vidotto, F. Rice Production in Europe. In *Rice Production Worldwide*; Chauhan, B.S., Jabran, K., Mahajan, G., Eds.; Springer International Publishing: Cham, Switzerland, 2017; pp. 93–116. ISBN 978-3-319-47514-1.
6. Mirmohamadsadeghi, S.; Karimi, K. Recovery of silica from rice straw and husk. In *Current Developments in Biotechnology and Bioengineering*; Elsevier: Amsterdam, The Netherlands, 2020; pp. 411–433. ISBN 978-0-444-64321-6.
7. Meng, H.; Nie, C.; Li, W.; Duan, X.; Lai, B.; Ao, Z.; Wang, S.; An, T. Insight into the effect of lignocellulosic biomass source on the performance of biochar as persulfate activator for aqueous organic pollutants remediation: Epicarp and mesocarp of citrus peels as examples. *J. Hazard. Mater.* **2020**, *399*, 123043. [[CrossRef](#)]
8. Kemmou, L.; Frontistis, Z.; Vakros, J.; Manariotis, I.D.; Mantzavinos, D. Degradation of antibiotic sulfamethoxazole by biochar-activated persulfate: Factors affecting the activation and degradation processes. *Catal. Today* **2018**, *313*, 128–133. [[CrossRef](#)]
9. Carvalho, I.T.; Santos, L. Antibiotics in the aquatic environments: A Review of the european scenario. *Environ. Int.* **2016**, *94*, 736–757. [[CrossRef](#)] [[PubMed](#)]
10. Prestinaci, F.; Pezzotti, P.; Pantosti, A. Antimicrobial resistance: A global multifaceted phenomenon. *Pathog. Glob. Health* **2015**, *109*, 309–318. [[CrossRef](#)] [[PubMed](#)]
11. Danner, M.-C.; Robertson, A.; Behrends, V.; Reiss, J. Antibiotic pollution in surface fresh waters: Occurrence and effects. *Sci. Total. Environ.* **2019**, *664*, 793–804. [[CrossRef](#)] [[PubMed](#)]
12. Wang, J.; Zhuan, R.; Chu, L. The occurrence, distribution and degradation of antibiotics by ionizing radiation: An overview. *Sci. Total. Environ.* **2019**, *646*, 1385–1397. [[CrossRef](#)]
13. Lykoudi, A.; Frontistis, Z.; Vakros, J.; Manariotis, I.D.; Mantzavinos, D. Degradation of sulfamethoxazole with persulfate using spent coffee grounds biochar as activator. *J. Environ. Manag.* **2020**, *271*, 111022. [[CrossRef](#)] [[PubMed](#)]
14. Schott, H.; Astigarrabia, E. Isoelectric points of some sulfonamides: Determination by microelectrophoresis and by calculations involving acid–Base strength. *J. Pharm. Sci.* **1988**, *77*, 918–920. [[CrossRef](#)]
15. Avisar, D.; Primor, O.; Gozlan, I.; Mamane, H. Sorption of sulfonamides and tetracyclines to montmorillonite clay. *Water Air Soil Pollut* **2010**, *209*, 439–450. [[CrossRef](#)]
16. Rauseo, J.; Barra Caracciolo, A.; Spataro, F.; Visca, A.; Ademollo, N.; Pescatore, T.; Grenni, P.; Patrolecco, L. Effects of sulfamethoxazole on growth and antibiotic resistance of a natural microbial community. *Water* **2021**, *13*, 1262. [[CrossRef](#)]
17. Xie, B.; Tang, X.; Ng, H.Y.; Deng, S.; Shic, X.; Song, W.; Huang, S.; Li, G.; Liang, H. Biological sulfamethoxazole degradation along with anaerobically digested centrate treatment by immobilized microalgal-bacterial consortium: Performance, mechanism and shifts in bacterial and microalgal communities. *Chem. Eng. J.* **2020**, *388*, 124217. [[CrossRef](#)]

18. Wang, J.; Zhuan, R. Degradation of antibiotics by advanced oxidation processes: An overview. *Sci. Total. Environ.* **2020**, *701*, 135023. [[CrossRef](#)]
19. Liu, S.; Peng, W.; Sun, H.; Wang, S. Physical and chemical activation of reduced graphene oxide for enhanced adsorption and catalytic oxidation. *Nanoscale* **2014**, *6*, 766–771. [[CrossRef](#)]
20. Duan, X.; Sun, H.; Tade, M.; Wang, S. Metal-free activation of persulfate by cubic mesoporous carbons for catalytic oxidation via radical and nonradical processes. *Catal. Today* **2018**, *307*, 140–146. [[CrossRef](#)]
21. Fang, G.; Liu, C.; Gao, J.; Dionysiou, D.D.; Zhou, D. Manipulation of persistent free radicals in biochar to activate persulfate for contaminant degradation. *Environ. Sci. Technol.* **2015**, *49*, 5645–5653. [[CrossRef](#)]
22. Manariotis, I.D.; Fotopoulou, K.N.; Karapanagioti, H.K. Preparation and characterization of biochar sorbents produced from malt spent rootlets. *Ind. Eng. Chem. Res.* **2015**, *54*, 9577–9584. [[CrossRef](#)]
23. Ntzoufra, P.; Vakros, J.; Frontistis, Z.; Tsatsos, S.; Kyriakou, G.; Kennou, S.; Manariotis, I.D.; Mantzavinos, D. Effect of sodium persulfate treatment on the physicochemical properties and catalytic activity of biochar prepared from spent malt rootlets. *J. Environ. Chem. Eng.* **2021**, *9*, 105071. [[CrossRef](#)]
24. Huong, P.T.; Jitae, K.; Al Tahtamouni, T.M.; Le Minh Tri, N.; Kim, H.-H.; Cho, K.H.; Lee, C. Novel activation of peroxymonosulfate by biochar derived from rice husk toward oxidation of organic contaminants in wastewater. *J. Water Process Eng.* **2020**, *33*, 101037. [[CrossRef](#)]
25. Li, F.; Duan, F.; Ji, W.; Gui, X. Biochar-Activated persulfate for organic contaminants removal: Efficiency, mechanisms and influencing factors. *Ecotoxicol. Environ. Saf.* **2020**, *198*, 110653. [[CrossRef](#)]
26. Prasad, C.S.; Maiti, K.N.; Venugopal, R. Effect of rice husk ash in whiteware compositions. *Ceram. Int.* **2001**, *27*, 629–635. [[CrossRef](#)]
27. Magioglou, E.; Frontistis, Z.; Vakros, J.; Manariotis, I.D.; Mantzavinos, D. Activation of Persulfate by Biochars from Valorized Olive Stones for the Degradation of Sulfamethoxazole. *Catalysts* **2019**, *9*, 419. [[CrossRef](#)]
28. Kaczmarczyk, B. FTIR study of conjugation in selected aromatic polyazomethines. *J. Mol. Struct.* **2013**, *1048*, 179–184. [[CrossRef](#)]
29. Zeng, M.; Shah, S.A.; Huang, D.; Parviz, D.; Yu, Y.H.; Xuezheng Wang, X.; Micah, J.; Green, M.J.; Cheng, Z. Aqueous exfoliation of graphite into graphene assisted by sulfonyl graphene quantum dots for photonic crystal applications. *ACS Appl. Mater. Interfaces* **2017**, *9*, 30797–30804. [[CrossRef](#)]
30. Andrade, T.S.; Vakros, J.; Mantzavinos, D.; Lianos, P. Biochar obtained by carbonization of spent coffee grounds and its application in the construction of an energy storage device. *Chem. Eng. J. Adv.* **2020**, *4*, 100061. [[CrossRef](#)]
31. Cho, D.W.; Yoon, K.; Kwon, E.E.; Biswas, J.K.; Song, H. Fabrication of magnetic biochar as a treatment medium for As(V) via pyrolysis of FeCl<sub>3</sub>-pretreated spent coffee ground. *Environ. Pollut.* **2017**, *229*, 942–949. [[CrossRef](#)]
32. Niu, H.Y.; Liu, S.L.; Cai, Y.Q.; Wu, F.C.; Zhao, X.L. MOF derived porous carbon supported Cu/Cu<sub>2</sub>O composite as high performance non-noble catalyst. *Microporous Mesoporous Mater.* **2016**, *219*, 48–53. [[CrossRef](#)]
33. Ntaflou, M.; Vakros, J. Transesterification activity of modified biochars from spent malt rootlets using triacetin. *J. Clean. Prod.* **2020**, *259*, 120931. [[CrossRef](#)]
34. Vakros, J. Biochars and their use as transesterification catalysts for biodiesel production: A short review. *Catalysts* **2018**, *8*, 562. [[CrossRef](#)]
35. Qian, L.; Guo, F.; Jia, X.; Zhan, Y.; Zhou, H.; Jiang, X.; Tao, C. Recent development in the synthesis of agricultural and forestry biomass-derived porous carbons for supercapacitor applications: A review. *Ionics* **2020**, *26*, 3705–3723. [[CrossRef](#)]
36. Gao, G.; Cheong, L.-Z.; Wang, D.; Shen, C. Pyrolytic carbon derived from spent coffee grounds as anode for sodium-ion batteries. *Carbon Resour. Convers.* **2018**, *1*, 104–108. [[CrossRef](#)]
37. Vakros, J.; Manariotis, I.D.; Dracopoulos, V.; Mantzavinos, D.; Lianos, P. Biochar from spent malt rootlets and its application to an energy conversion and storage device. *Chemosensors* **2021**, *9*, 57. [[CrossRef](#)]
38. Vakros, J.; Kordulis, C.; Lycourghiotis, A. Potentiometric mass titrations: A quick scan for determining the point of zero charge. *Chem. Comm.* **2002**, 1980–1981. [[CrossRef](#)] [[PubMed](#)]
39. Ataloglou, T.; Bourikas, K.; Vakros, J.; Kordulis, C.; Lycourghiotis, A. Kinetics of adsorption of the cobalt ions on the “Electrolytic Solution/ $\gamma$ -Alumina” interface. *J. Phys. Chem. B* **2005**, *109*, 4599–4607. [[CrossRef](#)]
40. Hu, S.; Xiang, J.; Sun, L.; Xu, M.; Qiu, J.; Fu, P. Characterization of char from rapid pyrolysis of rice husk. *Fuel Process. Technol.* **2008**, *89*, 1096–1105. [[CrossRef](#)]
41. Zhu, K.; Wang, X.; Geng, M.; Chen, D.; Lin, H.; Zhang, H. Catalytic oxidation of clofibric acid by peroxydisulfate activated with wood-based biochar: Effect of biochar pyrolysis temperature, performance and mechanism. *Chem. Eng. J.* **2019**, *374*, 1253–1263. [[CrossRef](#)]
42. Zhu, S.; Huang, X.; Ma, F.; Wang, L.; Duan, X.; Wang, S. Catalytic removal of aqueous contaminants on n-doped graphitic biochars: Inherent roles of adsorption and nonradical mechanisms. *Environ. Sci. Technol.* **2018**, *52*, 8649–8658. [[CrossRef](#)]
43. Ho, S.-H.; Chen, Y.; Li, R.; Zhang, C.; Ge, Y.; Cao, G.; Ma, M.; Duan, X.; Wang, S.; Ren, N. N-Doped graphitic biochars from c-phycocyanin extracted spirulina residue for catalytic persulfate activation toward nonradical disinfection and organic oxidation. *Water Res.* **2019**, *159*, 77–86. [[CrossRef](#)]
44. Qi, Y.; Ge, B.; Zhang, Y.; Jiang, B.; Wang, C.; Akram, M.; Xu, X. Three-Dimensional porous graphene-like biochar derived from enteromorpha as a persulfate activator for sulfamethoxazole degradation: Role of graphitic N and radicals transformation. *J. Hazard. Mater.* **2020**, *399*, 123039. [[CrossRef](#)]

45. Shen, B.; Liu, Y.; Liu, S.; Tan, X.; Zhang, P.; Du, L.; Wen, J. Catalytic degradation of sulfamethoxazole by persulfate activated with magnetic graphitized biochar: Multiple mechanisms and variables effects. *Process Saf. Environ. Prot.* **2020**, *144*, 143–157. [[CrossRef](#)]
46. Du, L.; Xu, W.; Liu, S.; Li, X.; Huang, D.; Tan, X.; Liu, Y. Activation of persulfate by graphitized biochar for sulfamethoxazole removal: The roles of graphitic carbon structure and carbonyl group. *J. Colloid Interface Sci.* **2020**, *577*, 419–430. [[CrossRef](#)] [[PubMed](#)]
47. Yin, R.; Guo, W.; Wang, H.; Du, J.; Wu, Q.; Chang, J.-S.; Ren, N. Singlet oxygen-Dominated peroxydisulfate activation by sludge-derived biochar for sulfamethoxazole degradation through a nonradical oxidation pathway: Performance and mechanism. *Chem. Eng. J.* **2019**, *357*, 589–599. [[CrossRef](#)]
48. Zhao, Y.; Yuan, X.; Li, X.; Jiang, L.; Wang, H. Burgeoning prospects of biochar and its composite in persulfate-Advanced oxidation process. *J. Hazard. Mater.* **2021**, *409*, 124893. [[CrossRef](#)] [[PubMed](#)]
49. Ren, W.; Xiong, L.; Yuan, X.; Yu, Z.; Zhang, H.; Duan, X.; Wang, S. Activation of peroxydisulfate on carbon nanotubes: Electron-Transfer mechanism. *Environ. Sci. Technol.* **2019**, *53*, 14595–14603. [[CrossRef](#)] [[PubMed](#)]
50. Yu, J.; Tang, L.; Pang, Y.; Zeng, G.; Wang, J.; Deng, Y.; Liu, Y.; Feng, H.; Chen, S.; Ren, X. Magnetic nitrogen-Doped sludge-derived biochar catalysts for persulfate activation: Internal electron transfer mechanism. *Chem. Eng. J.* **2019**, *364*, 146–159. [[CrossRef](#)]
51. Grilla, E.; Vakros, J.; Konstantinou, I.; Manariotis, I.D.; Mantzavinos, D. Activation of persulfate by biochar from spent malt rootlets for the degradation of trimethoprim in the presence of inorganic ions. *J. Chem. Technol. Biotechnol.* **2020**, *95*, 2348–2358. [[CrossRef](#)]
52. Cao, M.; Hou, Y.; Zhang, E.; Tu, S.; Xiong, S. Ascorbic acid induced activation of persulfate for pentachlorophenol degradation. *Chemosphere* **2019**, *229*, 200–205. [[CrossRef](#)]
53. Chen, J.; Yu, X.; Li, C.; Tang, X.; Sun, Y. Removal of tetracycline via the synergistic effect of biochar adsorption and enhanced activation of persulfate. *Chem. Eng. J.* **2020**, *382*, 122916. [[CrossRef](#)]
54. Guo, Y.; Zeng, Z.; Liu, Y.; Huang, Z.; Cui, Y.; Yang, J. One-Pot synthesis of sulfur doped activated carbon as a superior metal-free catalyst for the adsorption and catalytic oxidation of aqueous organics. *J. Mater. Chem. A* **2018**, *6*, 4055–4067. [[CrossRef](#)]
55. Hayat, W.; Zhang, Y.; Hussain, I.; Huang, S.; Du, X. Comparison of radical and non-radical activated persulfate systems for the degradation of imidacloprid in water. *Ecotoxicol. Environ. Saf.* **2020**, *188*, 109891. [[CrossRef](#)] [[PubMed](#)]
56. Özkal, C.B.; Frontistis, Z.; Antonopoulou, M.; Konstantinou, I.; Mantzavinos, D.; Meriç, S. Removal of Antibiotics in a Parallel-Plate Thin-Film-Photocatalytic Reactor: Process Modeling and Evolution of Transformation by-Products and Toxicity. *J. Environ. Sci.* **2017**, *60*, 114–122. [[CrossRef](#)] [[PubMed](#)]
57. Bourikas, K.; Vakros, J.; Kordulis, C.; Lycourghiotis, A. Potentiometric Mass Titrations: Experimental and Theoretical Establishment of a New Technique for Determining the Point of Zero Charge (PZC) of Metal (Hydr)Oxides. *J. Phys. Chem. B* **2003**, *107*, 9441–9451. [[CrossRef](#)]